

Cross-Field Ion Transport and Heating Due to Parametric Decay of Lower Hybrid Waves

R. McWilliams, D. N. Hill, N. S. Wolf,^(a) and N. Rynn

Department of Physics, University of California, Irvine, California 92717

(Received 5 October 1982)

Parametric decay of lower hybrid pump waves into daughter lower hybrid waves and electrostatic ion-cyclotron waves was observed above instability threshold power levels in a fully ionized plasma. The ion velocity distribution function was measured in time and space by the nonperturbing techniques of laser-induced fluorescence and ion optical tagging. Significant ion heating, T_i up to $6T_{i0}$, and cross-field transport were observed in the regime $\omega_0 \gtrsim 12\omega_{pi}$.

PACS numbers: 52.50.Gj

Many experiments that study the interaction of radio-frequency waves with plasmas are reaching power levels where the interaction of waves and particles can produce hot ions via nonlinear mechanisms. Previous works in the regime where the rf pump frequency lies between the ion and the electron cyclotron frequencies (e.g., ACT-1,¹ Alcator A,² ATC,³ Doublet IIA,⁴ H-1^{5,6} JFT-2,⁷ PETULA,⁸ and WEGA⁹) show evidence of the parametric decay instability. There is concern that nonlinear interactions, such as ponderomotive effects¹⁰ or parametric processes at the edge of plasmas, can reduce the amount of wave energy available to ions in the plasma core. On the other hand, parametric processes which occur in the plasma core may provide useful ion heating.¹¹

In this paper we present data showing significant changes in the ion distribution function in the presence of electrostatic ion-cyclotron waves driven parametrically by nearly electrostatic lower hybrid waves. In particular, using a recently developed nonperturbing laser diagnostic¹² we have been able to measure directly, for the first time, both the evolution of the ion distribution function, $f_i(\vec{x}, \vec{v}, t)$, and the trajectories of tagged ions in the presence of parametric decay. Substantial ion perturbations occurred only above the instability threshold. Three distinct effects were observed: (i) ion temperatures increased by as much as a factor of 6, (ii) cross-field diffusion was enhanced well above collisional levels, and (iii) an asymmetric ion velocity tail developed 0.4 msec after instability onset.

For the regime $\omega_{ci}, \omega_{pi} \ll \omega_0$, $\omega_2 \ll \omega_{pe} \ll \omega_{ce}$, where ω_0 is the pump wave frequency and ω_2 is the lower sideband frequency, the nearly electrostatic lower-hybrid-wave dispersion relation simplifies to $\omega \approx \omega_{pe} k_{\parallel} / k_{\perp}$, where k_{\parallel} (k_{\perp}) is the wave number parallel (perpendicular) to the confining magnetic field.¹³ Electrostatic ion-cyclo-

tron waves, $\omega \approx \omega_1$, follow the dispersion relation $\omega = \omega_{ci} + (T_e/T_i)\Gamma_1(k^2\rho_i^2)$, for $v_e \gg \omega/k_{\parallel} \gg v_i$, where v_e (v_i) is the electron (ion) thermal speed, $(2T_e/m_e)^{1/2}$, and $\Gamma_1(x) = e^{-x}I_1(x)$. The theory of parametric decay¹⁴ has been applied to lower hybrid waves by several authors¹⁵⁻¹⁸ for a dipole pump approximation, $\vec{k}_0 = 0$, and some finite pump effects.¹⁸ From Wong, Wilson, and Porkolab¹⁹ we estimate the parametric coupling coefficient to be dominated by the $\vec{E} \times \vec{B}$ drift. The decay threshold is modified also by convection.²⁰

The experiments reported here were performed in a single-ended Q machine²¹ (see Fig. 1) which provided a low-density ($5 \times 10^9 \leq n_e \leq 2 \times 10^{10} \text{ cm}^{-3}$), low-temperature ($T_i \approx T_e \approx 0.2 \text{ eV}$), nearly completely ionized potassium, barium, and/or cesium plasma 1.0 m long and 5 cm in diameter. The confining magnetic field was 2–6 kG. The lower hybrid waves were launched from a slow-wave antenna consisting of eight coaxial loops²² with the 30-MHz pump signal applied to the loops so that unidirectional waves of principal wavelength 12 cm were launched. Plasma density was estimated both from the angle of propagation of the pump wave with respect to \vec{B}_0 ($\theta \approx \omega/\omega_{pe}$) and from a Langmuir probe. Electron temperature was estimated with a Langmuir probe. The radial

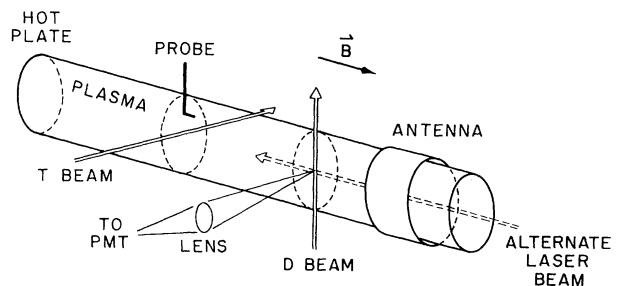


FIG. 1. Schematic of experiment showing laser-beam geometry. Antenna launches waves towards hot plate.

wavelength and resonance cone width were measured and found to be consistent with the dispersion relation.²²

Ion velocity distributions were measured with use of laser-induced fluorescence¹² (LIF), which uses a tunable dye laser to induce transitions to an excited state of the target plasma ion. The laser beam, collimated to 1 mm diameter, entered the plasma either perpendicular or parallel to the magnetic field (Fig. 1). Thus, both $f(\vec{v} \perp \vec{B})$ and $f(\vec{v} \parallel \vec{B})$ could be measured. The velocity resolution for either case was limited only by the natural linewidth of the absorption line, corresponding to an uncertainty of 10^3 cm/sec, or $0.03 v_{th}$ for cold ions ($T_i \approx 0.2$ eV).

In Fig. 2 we show the fundamental elements which identify the ion-cyclotron waves and daughter lower hybrid waves as resulting from the parametric decay of the pump wave. Frequency conservation is well satisfied, as demonstrated by Fig. 2(a), in which we plot the daughter wave

frequencies (actually ω_1 and $\omega_0 - \omega_2$) versus magnetic field. Qualitatively, the Manley-Rowe condition¹⁴ also was satisfied. The ion waves follow $\omega_i \approx l(1 + \delta_i)\omega_{ci}$ with $\delta_{i+1} < \delta_i$ [$l \leq 4$ in Fig. 2(a); we commonly observed $l \leq 7$ in the experiment]. Hence, this decay does not resemble a cascade pump depletion. Although not shown in the figure, the spectral width of the ion wave fundamental $\Delta\omega_1/\omega_1 \approx 0.36$ at full width at half maximum, and interferograms of the waves yielded phase information for less than one wavelength, possibly because of the spectral width and substantial wave damping.

Figure 2(b) shows the ion wave amplitude and ion temperature (obtained by fitting a Maxwellian to the steady-state distribution) versus pump power at different densities and magnetic fields. We estimate from Wong, Wilson, and Porkolab¹⁹ that the threshold of the rightmost amplitude curve should be 6 dB higher than that of the leftmost, while the experiment shows a 4 dB increase. It is also apparent from Fig. 2(b) that strong ion heating is observed only above the threshold power level of the parametric decay instability. This is not surprising, as the pump wave, whose energy resides in perpendicular field energy and parallel electron kinetic energy, does not interact significantly with the ions for two reasons: the wave phase velocity is substantially above the ion thermal velocity and the energy-transfer time from collisionally heated electrons to ions is longer than an ion transit time in the device (≈ 2 ms).

The change in the perpendicular ion temperature, T_y , versus time is shown in Fig. 3(a). The ion velocity distribution was measured immediately after shutoff of the variable-pulse-length pump signal. In general, T_y was found to increase linearly in time until an equilibrium was reached after approximately 1.6 msec. We also show the temperature decay after shutoff of a 1.6-msec rf pulse. The decay is consistent with axial convection of cold ions into and heated ions out of the plasma column. The complete $f(v_y)$ as a function of pulse length of the pump wave is shown in Fig. 3(b). The ion velocity distribution function starts out as a cold Maxwellian with equal parallel and perpendicular temperatures. Subsequently, substantial heating occurs, with an asymmetry developing in about 400 μ sec. Under circumstances where the perpendicular ion temperature was increased by as much as sixfold, there was observed to be less than a 25% increase in the parallel temperature, consistent with collisionless

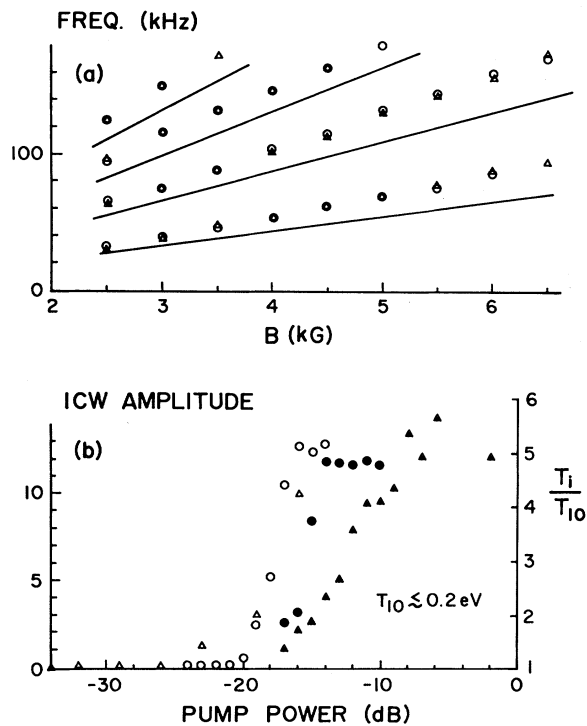


FIG. 2. (a) Frequency matching: triangles, ion waves; circles, daughter lower hybrid waves. Solid lines, $l\omega_{ci}$. (b) Ion wave amplitude and ion temperature vs rf power, showing instability threshold and ion heating only above threshold. -20 dB = 0.5 W. Open symbols: $B = 3$ kG, $n = 6 \times 10^9$ cm⁻³. Closed symbols: $B = 6$ kG, $n = 1.4 \times 10^{10}$ cm⁻³. Circles, ion wave amplitude, arbitrary units. Triangles, perpendicular ion temperature.

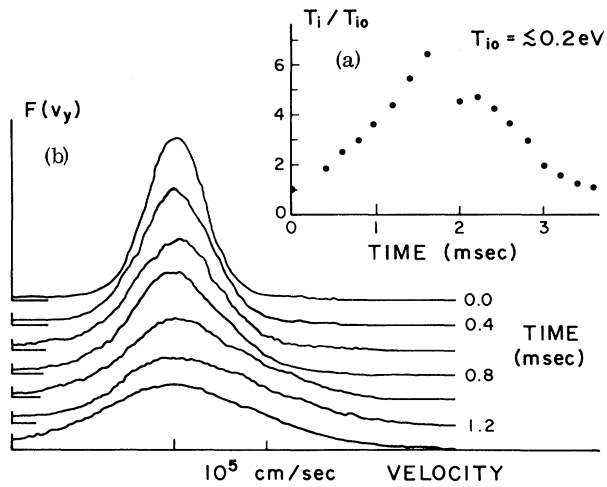


FIG. 3. Time-resolved ion distributions. (a) Ion temperature vs time for 1.6-msec rf pulse. (b) $f(v_y)$ vs rf pulse length. (Pump power = -9 dB.)

transfer of ion wave energy to the ions. The initial ion heating rate for the data in Fig. 3 is 5.8×10^{-3} eV per ion cyclotron period. From kinetic theory²³ we calculate

$$\frac{\partial T_{\perp}}{\partial(\omega_{ci} t)} \approx \left[4\pi^{1/2} \frac{T_{\perp}}{T_e} \left(\frac{\omega_{pi}}{\omega_{ci}} \right)^4 \sum_{i=1}^7 \left(\frac{\delta n}{n} \right)_i^2 J_i \right] T_{\perp}, \quad (1)$$

where J_i is essentially a Maxwellian integrated over weakly-Landau-damped resonant particles. From Eq. (1) a heating rate of 8×10^{-3} eV per ion cyclotron period is found for the experiment. Scaling Eq. (1) to the WEGA⁹ regime yields a predicted heating rate of 15 eV/msec, only slightly larger than the observed value. For Alcator A² the predicted heating rate is 26 eV/msec, whereas Schuss²⁴ notes that a ripple-trapped ion tail of energies above 5 keV occurred in less than 1 msec.

Measurements of cross-field ion motion were made with the technique of optical tagging.²⁵ Essentially, barium ions are tagged optically when they pass through the laser beam labeled T in Fig. 1, which optically pumps them to a long-lived quantum level L . A second laser beam (labeled D), spatially separated from the first by 18.5 cm along the magnetic field and which is tuned to produce fluorescence from ions in state L , is used to detect the tagged ions. By translating the location of the D -beam optics in a plane perpendicular to \vec{B} , cross-field ion motion can be followed. Typical results of such a measure-

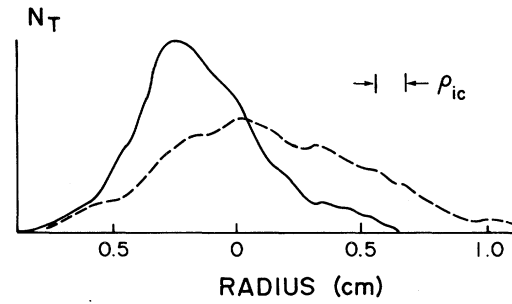


FIG. 4. Ion transport measurement. Number density of tagged ions vs radial position. Solid curve, no rf. Dashed curve, rf on, pump power at threshold.

ment are reproduced in Fig. 4, where we show the number density of tagged ions versus radial position of the detection optics for two different rf levels, above and below threshold. Below threshold (solid curve) the full width at half maximum corresponds to instrumental resolution, the finite gyroradius ρ_{ic} (1.2 mm) of the cold ions, and effects from the tagging geometry. So, we presently cannot interpret data for diffusion coefficients less than $D_{\perp} \approx 80 \text{ cm}^2/\text{sec}$, which is greater than the expected collisional coefficients (self-diffusion and ion-electron). The dashed curve (rf power just above threshold at beam D , but well above threshold in the focal region near beam T) shows enhancement of cross-field transport by $\delta D_{\perp} \approx 70 \text{ cm}^2/\text{sec}$. Cross-field transport was observed to increase with increasing rf power to the point where, for power levels 10 dB above threshold, cross-field diffusion was enhanced by $\delta D_{\perp} \approx 480 \text{ cm}^2/\text{sec}$. After Dupree,²⁶ at these power levels the diffusion enhancement might go as $\delta D_{\perp} \approx cT\bar{n}/\sqrt{2}eBn$. With use of \bar{n}/n of about 5% for 10 dB above threshold this predicts $\delta D_{\perp} \approx 120 \text{ cm}^2/\text{sec}$. Our estimate of \bar{n}/n is probably low as it was measured at the beam D and not over the entire ion path from the beam T .

In summary, we have examined the parametric decay of lower hybrid waves into other lower hybrid waves and ion-cyclotron waves. With use of a newly developed laser-induced fluorescence diagnostic the time-resolved ion distribution function was measured, from which it is clear that substantial ion heating and asymmetries in the distribution function occur in the presence of this decay process. By following the trajectory of tagged ions we observe, in a direct manner, cross-field transport due to lower-hybrid-wave heating.

Illuminating discussions were held with Dr. Gary

Allen, Dr. Yung Mok, Dr. Jack Schuss, and Dr. Gerard Van Hoven. We thank R. Blair, R. Karim, M. Okubo, and V. Laul for laboratory assistance. This work was supported by the National Science Foundation under Grant No. PHY80-9800.

^(a)Permanent address: Department of Physics, Dickinson College, Carlisle, Pa. 17013.

¹K. L. Wong and M. Ono, *Phys. Rev. Lett.* **47**, 842 (1981).

²J. J. Schuss *et al.*, *Nucl. Fusion* **21**, 427 (1981).

³M. Porkolab *et al.*, *Phys. Rev. Lett.* **38**, 230 (1977).

⁴J. Lohr *et al.*, *Bull. Am. Phys. Soc.* **22**, 1163 (1977).

⁵S. Bernabei *et al.*, *Nucl. Fusion* **17**, 929 (1977).

⁶T. K. Chu, S. Bernabei, and R. W. Motley, *Phys. Rev. Lett.* **31**, 211 (1973).

⁷T. Imai *et al.*, *Phys. Rev. Lett.* **43**, 586 (1979).

⁸P. Briand *et al.*, in *Proceedings of the Seventh International Conference on Plasma Physics and Controlled Nuclear Fusion Research, Innsbruck, Austria, 1978* (International Atomic Energy Agency, Vienna, Austria, 1979), Vol. 1, p. 65.

⁹C. Gormezano *et al.*, in *Proceedings of the Third Topical Conference on rf Plasma Heating, Pasadena, California, 1978*, edited by R. Gould (Caltech, Pasadena, 1978), paper A3.

¹⁰R. McWilliams and N. S. Wolf, *Phys. Rev. A* **25**, 1247 (1982).

¹¹G. R. Allen *et al.*, *Phys. Rev. Lett.* **41**, 1045 (1978).

¹²R. A. Stern and J. A. Johnson, *Phys. Rev. Lett.* **34**, 1548 (1975); D. N. Hill, S. Fornaca, and M. G. Wickham, to be published.

¹³R. McWilliams and R. W. Motley, *Phys. Fluids* **24**, 2022 (1981).

¹⁴J. M. Manley and H. E. Rowe, *Proc. IRE* **44**, 904 (1956).

¹⁵R. L. Berger, Liu Chen, P. K. Kaw, and F. W. Perkins, *Phys. Fluids* **20**, 1864 (1977).

¹⁶P. K. Kaw, C. Z. Cheng, and Liu Chen, Princeton University Plasma Physics Laboratory Report No. PPPL-1305, 1976 (unpublished).

¹⁷M. Porkolab, *Nucl. Fusion* **18**, 367 (1978).

¹⁸M. Porkolab, *Phys. Fluids* **20**, 2058 (1977).

¹⁹K. L. Wong, J. R. Wilson, and M. Porkolab, *Phys. Fluids* **23**, 96 (1980).

²⁰D. Pesme, G. Laval, and R. Pellat, *Phys. Rev. Lett.* **31**, 203 (1973).

²¹N. Rynn, *Rev. Sci. Instrum.* **35**, 40 (1964).

²²P. M. Bellan and M. Porkolab, *Phys. Fluids* **19**, 995 (1976).

²³R. C. Davidson, *Methods in Nonlinear Plasma Theory* (Academic, New York, 1977).

²⁴J. J. Schuss, private communication.

²⁵R. A. Stern, D. N. Hill, and N. Rynn, *Phys. Lett.* **93A**, 127 (1983).

²⁶T. H. Dupree, *Phys. Fluids* **10**, 1049 (1967).

Mean-Field Theory for Diffusion-Limited Cluster Formation

M. Muthukumar

Institute for Theoretical Physics, University of California at Santa Barbara, Santa Barbara, California 93106, and Department of Chemistry, Illinois Institute of Technology, Chicago, Illinois 60616

(Received 3 December 1982)

A mean-field theory for the diffusion-controlled cluster formation is presented by considering the competition among the different portions of a growing cluster for the incoming diffusive particles. This competition is shown to introduce a screening length which depends inversely on the density of the cluster. The Hausdorff dimensionality D of these clusters is shown to be $(d^2 + 1)/(d + 1)$ where d is the Euclidean dimensionality. This result is in excellent agreement with that of the computer simulations of Witten and Sander and of Meakin.

PACS numbers: 68.70.+w, 05.70.-a, 82.70.Dd

In an attempt to describe the growth of clusters of small particles, Witten and Sander¹ recently simulated a diffusion-limited aggregation in $d = 2$ on a computer and compared with other models such as Eden growth,² dendritic growth,³ random animals,⁴ and percolating clusters.⁵ Meakin⁶ also has independently performed simulations of diffusion-controlled cluster growth similar to those

of Witten and Sander for $d = 2, 3$, and 4. These simulations start with a single seed particle at the origin of a lattice. A second particle is added at some random site at a large distance from the origin. This particle undergoes a random walk on the lattice until it reaches a site adjacent to the seed and becomes part of the growing cluster. A third particle is then introduced at a random